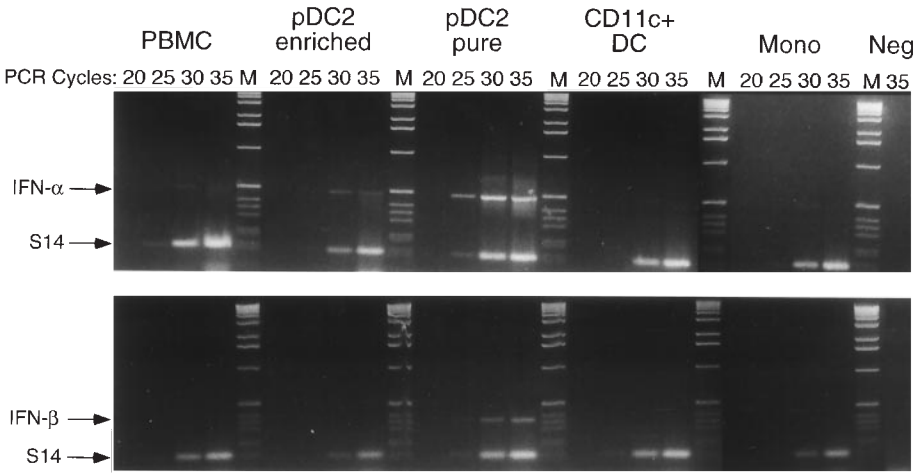

Fig. 3. RT-PCR amplification of IFN-α and IFN-β. PCR products amplified from each cell population after 20, 25, 30, or 35 cycles were separated on a 2% agarose gel containing ethidium bromide. Negative controls contained no cDNA. Marker is 1-kb DNA Ladder (Life Technologies, Grand Island, New York). IFN-α mRNA is apparent in PBMCs, is increased in the DC2 precursors (pDC2s) with enrichment and purification, and is diminished in the monocyte fraction. IFN-β mRNA is visualized only in the most highly purified DC2 precursors.

gen-presenting type 2 DCs upon terminal differentiation.

Type 1 IFNs have pleiotropic effects on the immune system, including up-regulation of MHC class I on all cell types and activation of macrophage and NK cells (*2*). IFNs are also critical in the activation and survival of both $CD4^+$ and $CD8^+$ T cells (*25*, *26*). Now with the ability to trace and isolate IPCs, it should be possible to directly study the interaction between IPCs and other cell types within the immune system. IFN-α has been widely used for treating hepatitis B and C as well as various cancers. A progressive loss of IPCs has been observed during HIV infection, suggesting that IPCs may represent targets for HIV-mediated infection and deletion. The present study provides an approach to directly monitor the number and functional state of IPCs in these patients. The ability to purify and culture IPCs in vitro will allow further studies on the molecular mechanisms that control the survival and growth of IPCs and their production of IFN, which may lead to novel therapies for patients with viral infections and cancer.

References and Notes

1. A. Isaacs and J. Lindemann, *Proc. R. Soc. London* **147**, 258 (1957).
2. P. Fitzgerald-Bocarsly, *Pharmacol. Ther.* **60**, 39 (1993).
3. H. Kirchner *et al.*, *Immunobiology* **156**, 65 (1979).
4. H. H. Peter *et al.*, *Eur. J. Immunol.* **10**, 547 (1980).
5. J. Abb, H. Abb, F. Deinhart, *Clin. Exp. Immunol.* **52**, 179 (1983).
6. B. Perussia, V. Fanning, G. Trinchieri, *Nat. Immun. Cell Growth Regul.* **4**, 120 (1985).
7. J. Chehimi *et al.*, *Immunology* **68**, 488 (1989).
8. K. Sandberg *et al.*, *Scand. J. Immunol.* **34**, 565 (1991).
9. S. E. Starr *et al.*, *Adv. Exp. Med. Biol.* **329**, 173 (1993).
10. H. Svensson *et al.*, *Scand. J. Immunol.* **44**, 164 (1996).
11. S. B. Feldman *et al.*, *Virology* **204**, 1 (1994).
12. M. Feldman and P. Fitzgerald-Bocarsly, *J. Interferon Res.* **10**, 435 (1990).
13. J. J. Ferbas *et al.*, *J. Immunol.* **152**, 4649 (1994); S. B. Feldman *et al.*, *J. Leukocyte Biol.* **57**, 214 (1995).
14. S. Ghanekar *et al.*, *J. Immunol.* **157**, 4028 (1996).
15. C. Lopez, P. Fitzgerald, F. P. Siegal. *J. Infect. Dis.* **148**, 962 (1983); D. M. Howell, S. B. Feldman, P. Kloser, P. Fitzgerald-Bocarsly, *Clin. Immunol. Immunopathol.* **7**, 223 (1994); J. Ferbas, J. Navratil, A. Logar, C. Rinaldo, *Clin. Diagn. Lab. Immunol.* **2**, 138 (1995).
16. F. P. Siegal *et al.*, *J. Clin. Invest.* **78**, 115 (1986).
17. U. O'Doherty *et al.*, *J. Exp. Med.* **178**, 1067 (1993).
18. U. O'Doherty *et al.*, *Immunology* **82**, 487 (1994).
19. G. Grouard *et al.*, *J. Exp. Med.* **185**, 1101 (1997).
20. J. Olweus *et al.*, *Proc. Natl. Acad. Sci. U.S.A.* **94**, 12551 (1997).
21. M.-C. Rissoan *et al.*, *Science* **283**, 1183 (1999).
22. Cells were incubated with UV-irradiated HSV in quadruplicate wells (2×10^5 cells in 200 μl of culture medium per well with 2×10^4 plaque-forming units of virus in 96-well culture plates) (*23*). IFN in supernatants from 24-hour cultures with and without IL-3 were analyzed with cytopathic reduction in human foreskin fibroblast monolayers cultured with vesicular stomatitis virus (sensitivity, 2 to 25 IU of IFN per milliliter) (*23*). Cytocentrifuge preparations of cells from 6-hour cultures were prepared for IFN-α immunostaining with mouse monoclonal antibody 7N4-1 (10 μg/ml; Schering-Plough Research Institute, Kenilworth, NJ) (*21*). Cells from 6-hour cultures were centrifuged and the sediment frozen for IFN-α and IFN-β mRNA PCR analyses (*24*).
23. F. P. Siegal *et al.*, *Leukemia* **8**, 1474 (1994).
24. Reverse transcriptase (RT)–PCR: RNA was isolated with the acid guanidinium thiocyanate–phenol-chloroform method [P. Chomczrski and N. Sacchi, *Anal. Biochem.* **162**, 156 (1987)]. DNA contamination was removed by digestion with deoxyribonuclease I (5 U; Boehringer-Mannheim, Indianapolis, IN) for 30 min at 37°C. Controls without RT were performed. Reverse transcription was carried out with pd(T)12-18 (Pharmacia, Alameda, CA) priming and Superscript II RT (Life Technologies, Grand Island, NY). PCR reaction volume was 25 μl containing 100 ng of each primer, 40 nM of each deoxynucleoside triphosphate, 1 μl of cDNA, and 1.25 U of AmpliTaq (Perkin-Elmer, Foster City, CA). The primers used were as follows: IFN-α (sense: 5′-GATGGCCGTGCTGGTGCTCA-3′; antisense: 5′-TGATTTCTGCTCTGACAACCTCCC-3′; probe: 5′-CTCAAGCCATCTCTGTCCTCCATGAGATGA-3′); IFN-β (sense: 5′-TTGAATGGGAGGCTTGAATA-3′; antisense: 5′-CTATGGTCCAGGCACAGTGA-3′; probe: 5′-GGCTGGAATGAGACTATTGTTGAGAACCTC-3′); and human ribosomal protein S14 (sense: 5′-GGCAGACCGAGATGAATCCTCA-3′; antisense: 5′-CAGGTCCAGGGGTCTTGGTCC-3′). Each PCR amplification contained primers for the ribosomal protein S14, to verify the amounts of cDNA. A GeneAmp PCR System 9700 (Perkin-Elmer/Applied Biosystems) was used with an initial denaturation step of 94°C for 5 min, followed by cycles of 94°C for 30 s, 60°C for 30 s, 72°C for 60 s, and a final elongation step of 72°C for 7 min. PCR products were separated on a 2% agarose gel, followed by DNA blotting and hybridization with ^{32}P-labeled probes.
25. S. Sun *et al.*, *J. Exp. Med.* **188**, 2335 (1998).
26. P. Marrack *et al.*, *ibid.* **189**, 521 (1999).

27. We thank T. L. Nagabhushan, L. L. Lanier, H. Kanzler, D. Imperato, C. Lopez, L. Filgueira, G. Grouard, and R. Rai for continued support. F.P.S. is supported by a grant from Pharmacia and Upjohn. DNAX Research Institute of Molecular and Cellular Biology is supported by Schering-Plough Corporation.

8 February 1999; accepted 3 May 1999

Math1: An Essential Gene for the Generation of Inner Ear Hair Cells

Nessan A. Bermingham,[1,2] Bassem A. Hassan,[1,2] Steven D. Price,[7] Melissa A. Vollrath,[5] Nissim Ben-Arie,[2]* Ruth Anne Eatock,[5,6] Hugo J. Bellen,[1,2,4,5] Anna Lysakowski,[7] Huda Y. Zoghbi[1,2,3,4,5]†

The mammalian inner ear contains the cochlea and vestibular organs, which are responsible for hearing and balance, respectively. The epithelia of these sensory organs contain hair cells that function as mechanoreceptors to transduce sound and head motion. The molecular mechanisms underlying hair cell development and differentiation are poorly understood. *Math1*, a mouse homolog of the *Drosophila* proneural gene *atonal*, is expressed in inner ear sensory epithelia. Embryonic *Math1*-null mice failed to generate cochlear and vestibular hair cells. This gene is thus required for the genesis of hair cells.

The inner ear initially forms as a thickening of the ectoderm, termed the otic placode, between rhombomeres 5 and 6 in the hindbrain. The otic placode gives rise to neurons of the VIIIth cranial nerve and invaginates to become the otocyst, from which the inner ear

Downloaded from www.sciencemag.org on June 29, 2010

will develop. The mature mammalian inner ear comprises one auditory and five vestibular organs: the utricle, the saccule, and three semicircular canals (Fig. 1A). The sensory epithelia of these organs consist of mechanoreceptive hair cells, supporting cells, and nerve endings. Hair cells and supporting cells proliferate and differentiate within the sensory epithelia, with peak mitoses between embryonic day 13 (E13) and E18 in mice (*1*). Although several genes have been implicated in the development of the inner ear (*2*), none have been shown to be required specifically for the genesis of hair cells.

Hair cells and supporting cells arise from a common progenitor (*3*), but the mechanisms that specify fate are unknown. During myogenesis and neurogenesis, cell fate specification requires basic helix-loop-helix (bHLH) transcription factors (*4, 5*). *Math1* [mouse *atonal* (*ato*) homolog 1], a member of the bHLH family, is expressed in the hindbrain, dorsal spinal cord, and external germinal layer of the cerebellum

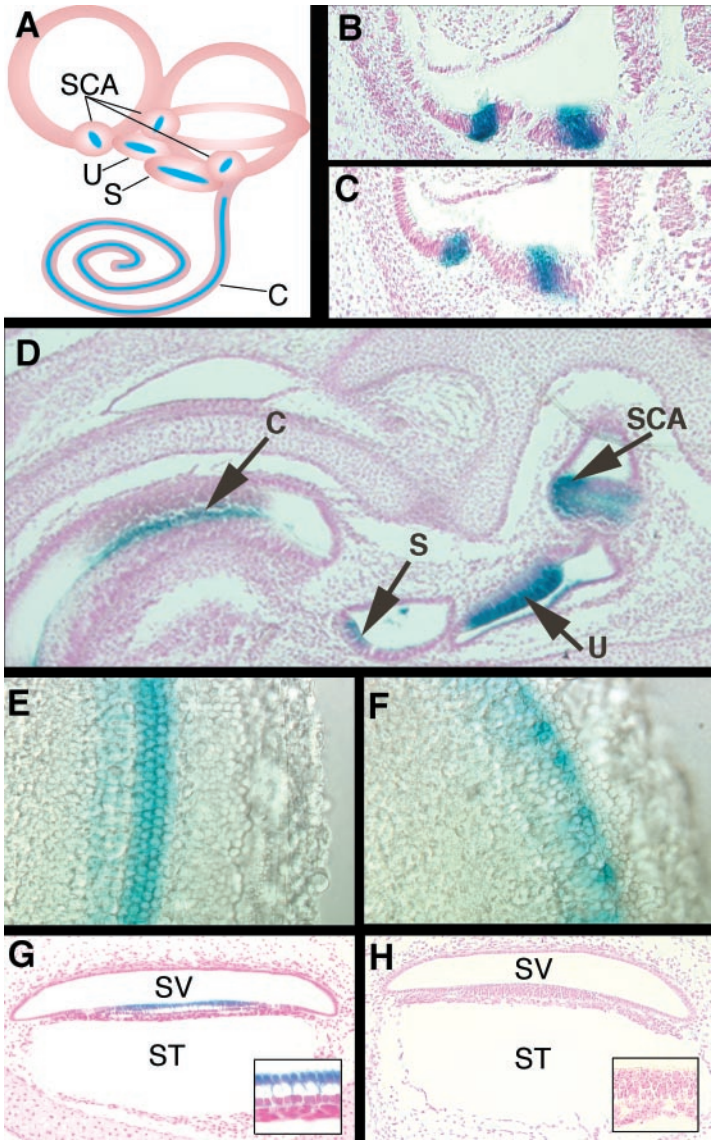

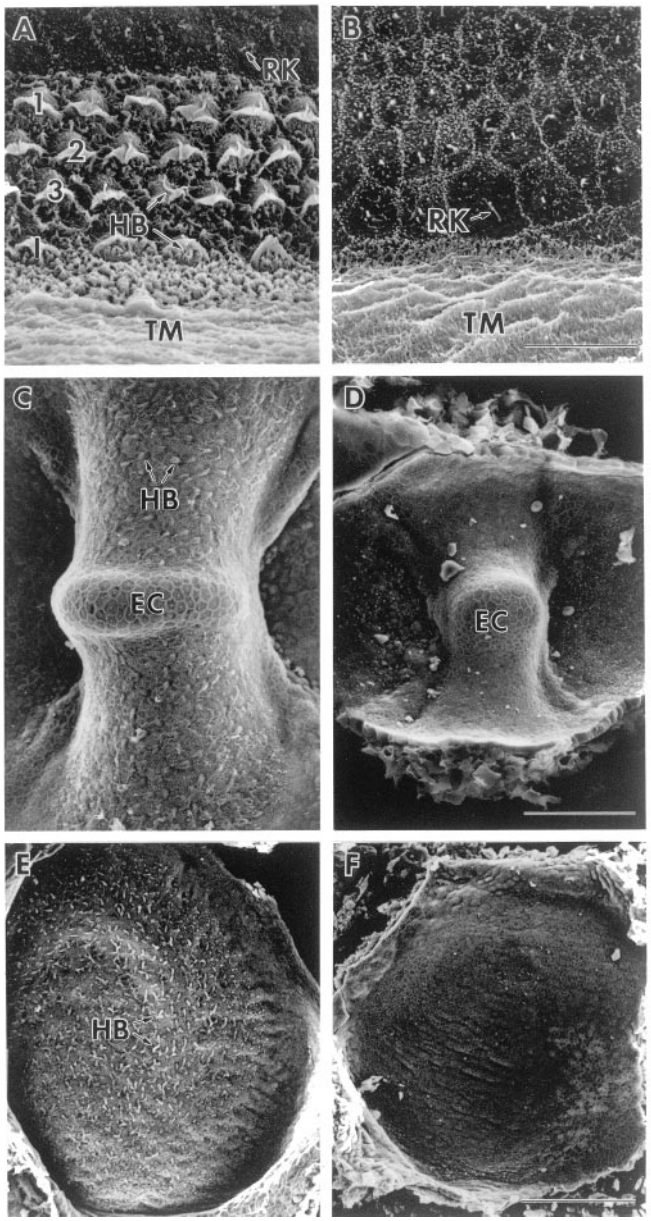

Fig. 1 (left). Inner ear β-Gal staining (blue) of (**B**, **D**, **E**, and **G**) *Math1*$^{+/\beta\text{-Gal}}$ and (**C**, **F**, and **H**) *Math1*$^{\beta\text{-Gal}/\beta\text{-Gal}}$ embryos. (**A**) Schematic of mature inner ear. Blue indicates location of sensory epithelium, cochlea (C), saccule (S), utricle (U), and semicircular canal ampullae (SCA). (B and C) β-Gal staining in the otic vesicle at E12.5 demonstrates that *Math1* is expressed before the differentiation of inner ear hair cells; (D) staining of an E14.5 inner ear demonstrates staining throughout the sensory organ epithelia. (E and F) Surface views at the middle turn of an E18.5 cochlea. There is positive staining of the three outer and one inner hair cell rows in (E) and nonspecific staining in (F). (G and H) Sections through the basal region of an E18.5 cochlea: scala vestibuli (SV) and scala tympani (ST). Insets show high magnification of the middle region of the organ of Corti and demonstrate the absence of hair cells. (G) Hair cells are deeply stained; (H) in the null mutant, hair cells are absent. Original magnifications are as follows: (B and C), ×100; (D), ×50; (E and F), ×630; (G and H), ×160; and insets in (G) and (H), ×400. **Fig. 2 (right).** Scanning electron micrographs of E18.5 inner ear sensory epithelia in wt and *Math1*$^{\beta\text{-Gal}/\beta\text{-Gal}}$ mice. (**A**, **C**, and **E**) Wild-type epithelia; (**B**, **D**, and **F**) null epithelia. (A and B) The organ of Corti of the cochlea at the middle turn. In wt mice, there are three rows of outer hair cells (1, 2, and 3), one row of inner hair cells (I), all with hair bundles (HB). The tectorial membrane (TM), an accessory structure of the cochlea, is seen at the bottom. Above the hair cells are nonspecialized epithelial cells with rudimentary kinocilia (RK). (B) In null mutants, there are only nonspecialized epithelial cells. (C and D) Crista ampullaris of a vertical semicircular canal. The null crista is similar to the wt crista in overall shape, including the septum (eminentia) cruciatum (EC), but is smaller and lacks hair cells. (E and F) The macula of the utricle. The null macula is smaller than the wt macula and lacks hair cells. Scale bars represent 10 μm in (A) and (B), 50 μm in (C) and (D), and 100 μm in (E) and (F).

Downloaded from www.sciencemag.org on June 29, 2010

(*6*–*8*). Mice that are heterozygous for a targeted deletion of *Math1* (*Math1*$^{+/-}$) are viable and appear normal, but *Math1*-null mice (*Math1*$^{-/-}$) die shortly after birth and lack cerebellar granule neurons (*8*). To detect subtle *Math1* expression patterns missed by RNA in situ hybridization, we generated a second *Math1*-null allele (*Math1*$^{\beta\text{-Gal}/\beta\text{-Gal}}$) by replacing the *Math1* coding region with β-galactosidase (β-Gal) (*9, 10*). *Math1*$^{\beta\text{-Gal}/\beta\text{-Gal}}$ mice showed all the phenotypic features reported in the *Math1*$^{-/-}$ mice (*8*). β-Gal expression in the cerebellum and dorsal spinal cord was identical to that of *Math1* (*10*). β-Gal was also expressed throughout the prospective sensory epithelia of the otic vesicle at E12.5 of both *Math1*$^{+/\beta\text{-Gal}}$ and *Math1*$^{\beta\text{-Gal}/\beta\text{-Gal}}$ embryos (Fig. 1, B and C). Expression was evident throughout the sensory epithelia of the utricle, saccule, semicircular canals, and cochlea at E14.5 (Fig. 1D). By E18.5, β-Gal was restricted to the hair cells of the developing sensory epithelia in *Math1*$^{+/\beta\text{-Gal}}$ mice (Fig. 1, E and G) (*11*). However, *Math1*$^{\beta\text{-Gal}/\beta\text{-Gal}}$ mice retained β-Gal expression in some supporting cell layers of the sensory epithelium. In the cochlea, β-Gal expression was absent in the basal turn (Fig. 1H), greatly decreased in the middle turn (Fig. 1F), and similar to heterozygotes in the apical turn at E18.5 (*12*), consistent with the basal to apical developmental gradient of the cochlea. Gross morphological analysis of the inner ear of *Math1*$^{\beta\text{-Gal}/\beta\text{-Gal}}$ mice at E18.5, 1 day before full gestation, revealed no obvious defects in overall structure compared with wild-type (wt) littermates. The branches of the VIIIth cranial nerve were present and reached the epithelia (*12*).

To examine the sensory epithelia, we excised utricles and cochleas of wt, *Math1*$^{+/\beta\text{-Gal}}$, and *Math1*$^{\beta\text{-Gal}/\beta\text{-Gal}}$ mice and viewed the sensory epithelia with Nomarski optics. Hair bundles were present in both organs of wt mice and heterozygotes but were completely absent in *Math1*-null littermates. Scanning electron microscopy (SEM) of the cochlea and vestibular organs confirmed the absence of hair bundles in null mice (Fig. 2) (*13*). To determine whether a lack of hair bundles reflects the absence of hair cells, we examined cross sections of the sensory epithelia of all inner ear organs, using both light microscopy (LM) and transmission electron microscopy (TEM). Sensory epithelia in null mice were considerably thinner, lacked the normal stratification of cell nuclei, and stained uniformly. All of this is consistent with the absence of hair cells (Fig. 3). TEM clearly distinguishes between hair cells and supporting cells in normal utricles: Hair cells have hair bundles, less electron-dense cytoplasm, more apical nuclei, and no secretory granules (*14*). The sensory epithelia of the null mutants lacked hair cells entirely but did have supporting cells with a normal appearance, including electron-dense cytoplasm, basal nuclei, and secretory granules (Fig. 4, A and B). In the cochlea, TEM analysis demonstrated the loss of hair cells as well (Fig. 4, C and D). In addition, there was no evidence of apoptotic cell death in the sensory epithelium by LM and TEM analysis.

The lack of hair cells at E18.5 may be due to a lack of sensory cell progenitors, the inability of progenitors to differentiate into hair cells, or the inability of hair cells to maintain the differentiated state (*15, 16*). The first possibility is unlikely because progenitors give rise to both hair cells and supporting cells (*3*), and supporting cells were present in *Math1*$^{\beta\text{-Gal}/\beta\text{-Gal}}$ mice. To test the remaining possibilities, we examined the expression of the hair cell–specific markers, myosin VI and calretinin. Both are expressed in differentiating hair cells (before hair bundle formation) and in mature vestibular and auditory hair cells, but not in supporting cells (*17*–*19*). Myosin VI is first detected at E13.5 in the developing inner ear (*16*), whereas calretinin is expressed 2 days later at E15.5 (*18*). Antibodies to myosin VI and calretinin were used to detect expression of these hair cell markers in wt and *Math1*$^{\beta\text{-Gal}/\beta\text{-Gal}}$ littermates. Myosin VI–positive cells were clearly visible in the developing otic vesicles of wt embryos but were completely absent in *Math1*$^{\beta\text{-Gal}/\beta\text{-Gal}}$ embryos (Fig. 5, A and B). Myosin VI staining was absent in the cochlea of E18.5 *Math1*-null mutants (*12*). Calretinin-positive cells were observed in the sensory epithelia of all E15.5 (*12*), E16.5 (Fig. 5, C through F), and E18.5 (Fig. 5, G and H) wt mice, but they were not observed in the sensory epithelia of *Math1*$^{\beta\text{-Gal}/\beta\text{-Gal}}$ mice (Fig. 5, C through H) (*20*). Given the basal to apical developmental gradient of the cochlea, we examined sections from basal, middle, and apical turns. Hair cells were lacking in all sections; representative sections from the middle turn are shown in Figs. 2 through 4. These data demonstrate that hair cells never developed within the sensory epithelia of *Math1*$^{\beta\text{-Gal}/\beta\text{-Gal}}$ mice. The presence of the tectorial and otolithic membranes [secreted in part by the supporting cells (*21, 22*)], together with the TEM results, indicates that the sensory epithelia of *Math1*$^{\beta\text{-Gal}/\beta\text{-Gal}}$ mice have functional supporting cells. Preliminary data from TEM and LM cross sections show apparent overcrowding of nuclei in the basal layers of the sensory epithelia of null mice, consistent with an increase in the number of supporting cells in the sensory epithelia (Fig. 4, C and D). This finding, together with the absence of apoptosis, raises the possibility that, in *Math1*$^{\beta\text{-Gal}/\beta\text{-Gal}}$ mice, there is a fate switch from hair cells to supporting cells.

Math1 is essential for hair cell development in the inner ear. Its expression pattern

[1]Howard Hughes Medical Institute, [2]Department of Molecular and Human Genetics, [3]Department of Pediatrics, [4]Developmental Biology Program, [5]Division of Neuroscience, [6]Bobby R. Alford Department of Otorhinolaryngology and Communicative Sciences, Baylor College of Medicine, Houston, TX 77030, USA. [7]Department of Anatomy and Cell Biology, University of Illinois at Chicago, Chicago, IL 60612, USA.

*Present address: Department of Cell and Animal Biology, Alexander Silberman Institute of Life Sciences, Hebrew University of Jerusalem, Givat-Ram, Jerusalem 91904, Israel.

†To whom correspondence should be addressed. E-mail: hzoghbi@bcm.tmc.edu

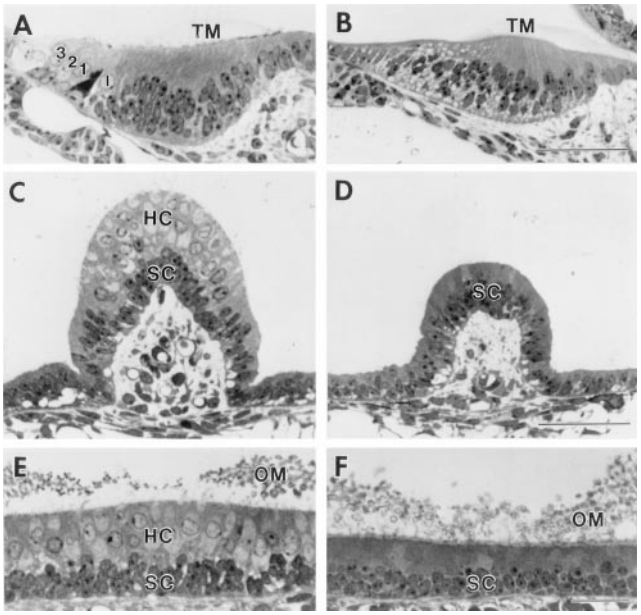

Fig. 3. Light micrographs of semithin transverse sections of inner ear sensory epithelia in (**A**, **C**, and **E**) wt and (**B**, **D**, and **F**) *Math1*$^{\beta\text{-Gal}/\beta\text{-Gal}}$ mice at E18.5. (A) In wt cochlea at the middle turn, three outer hair cells (1, 2, and 3) and one inner hair cell (I) are present, whereas (B) the null mutant cochlea has only epithelial cells in the same region. The tectorial membrane (TM) is seen at the top of (A) and (B). Hair cells (HC) and supporting cells (SC) are present in (C) the wt crista ampullaris and (E) utricular macula, but only supporting cells are present in (D) and (F) null mice. The crista was cut obliquely, accounting for the multiple layers of hair cells in (C). The otolithic membrane (OM), an accessory structure of the utricle, is present in both (E) wt and (F) null mice. Scale bars represent 100 μm in (A) and (B), 50 μm in (C) and (D), and 25 μm in (E) and (F).

Downloaded from www.sciencemag.org on June 29, 2010

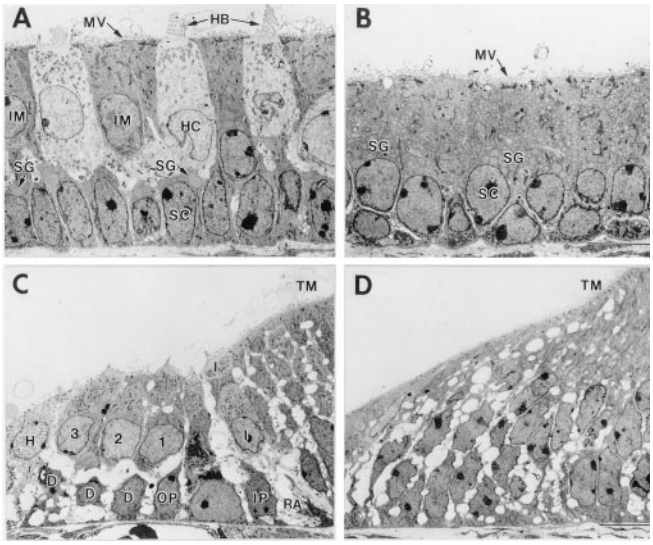

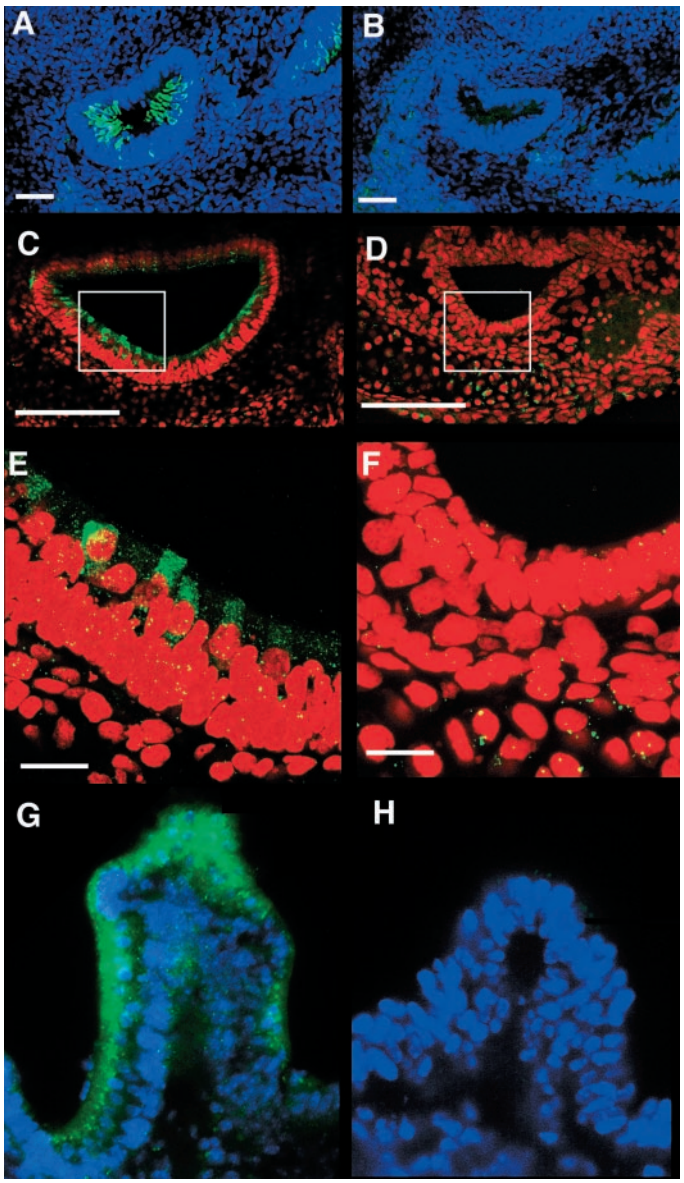

Fig. 4 (left). Transmission electron micrographs of E18.5 (**A** and **B**) utricular macula and (**C** and **D**) the middle turn of the cochlea in wt and null *Math1*$^{\beta\text{-Gal}/\beta\text{-Gal}}$ mice. Hair cells (HC) and supporting cells (SC) are present in (A) wt utricular macula, but only supporting cells are present in (B) null mice. Hair cells have hair bundles (HB); supporting cells have microvilli (MV). Hair cells are less electron dense and have more apical nuclei than supporting cells, but only the latter have secretory granules (SG). Some immature hair cells (IM) are evident in the wt mice. (C) In the wt cochlea, several cell types can be observed: outer hair cells (1, 2, and 3), inner hair cells (I), Deiter's cells (D), Hensen's cells (H), and inner (IP) and outer pillar (OP) cells. Radial afferents (RA) are seen approaching the base of the inner hair cell. The section is slightly oblique, and parts of two adjacent inner hair cells can be seen. (D) In the null cochlea, there are no obvious distinctions between cell types, with the possible exception of the cell at the far left, which may be a Hensen's cell. Both wt and null cochlea have a tectorial membrane (TM), which covers the supporting cells on the right of (C and D). Scale bars represent 10 μm. **Fig. 5 (right).** (**A** through **F**) Confocal and (**G** and **H**) immunofluorescence microscopy of (A, C, E, and G) wt and (B, D, F, and H) *Math1*$^{\beta\text{-Gal}/\beta\text{-Gal}}$ embryos. (A and B) Myosin VI immunostaining of an E13.5 vestibule. (C through F) Calretinin immunostaining of E16.5 utricles. (G and H) Calretinin immunostaining of E18.5 crista ampullaris. The crista is cut at an oblique angle, which accounts for the multiple layers of hair cells in (G). Immunostaining (green) with myosin VI and calretinin is evident in immature and mature hair cells of (A, C, E, and G) wt epithelia but is clearly absent in (B, D, F, and H) *Math1*$^{\beta\text{-Gal}/\beta\text{-Gal}}$ epithelia. Boxed areas in (C) and (D) indicate regions magnified in (E) and (F). Sections were counterstained with (A and B) TOTO-3 iodide or (C through F) propidium iodide for confocal microscopy and were counterstained with (G and H) DAPI for immunofluorescent microscopy. Scale bars represent 50 μm in (A) and (B), 100 μm in (C) and (D), and 15 μm in (E) and (F); original magnification is ×200 in (G) and (H).

and in vivo function are akin to those of *Math1*'s proneural homolog, *ato* (*23*). *ato* is expressed in a ring of epithelial cells within the antennal disc of *Drosophila*. Some of these cells will subsequently give rise to mechanoreceptors in the Johnston organ, which is necessary for hearing (*24*) and negative geotaxis (*25*). Mechanoreceptor progenitor cells are affected in *ato* mutants (*23*), whereas only the mechanoreceptors, and not their progenitors, are absent in *Math1*-null mice.

To our knowledge, *Math1* is the first gene shown to be required for the specification of hair cells. We propose that *Math1* acts as a "pro–hair cell gene" in the developing sensory epithelia. Three recent studies provide evidence supporting a lateral inhibition model for the determination of hair cells and supporting cells (*26*), in which the interplay of *Delta* and *Notch* homologs results in the selection of individual hair cells from clusters of competent cells. Such a model entails that the sensory epithelia express a pro–hair cell gene, whose function is essential for hair cell fate specification. *Math1* is a likely candidate for such a gene.

Finally, because ectopic expression of *ato* in the fruit fly (*23*) [and its homolog *Xath1* in *Xenopus* (*27*)] can recruit epithelial cells into specific neuronal fates, it should be possible to test whether expression of *Math1* in inner ear epithelia recruits hair cells. The potential clinical applications of such studies cannot be overlooked, because loss of hair cells through disease, trauma, and aging is a common cause of deafness and vestibular dysfunction.

References and Notes

1. R. J. Ruben, *Acta Oto-Laryngol. Suppl.* **220**, 1 (1967).
2. S. L. Mansour, J. M. Goddard, M. R. Capecchi, *Development* **117**, 13 (1993); M. Torres, E. Gomez-Pardo, P. Gruss, *ibid.* **122**, 3381 (1996); W. Wang, T. Van De Water, T. Lufkin, *ibid.* **125**, 621 (1998).
3. D. M. Fekete, S. Muthukumar, D. Karagogeos, *J. Neurosci.* **18**, 7811 (1998).
4. H. Weintraub *et al.*, *Science* **251**, 761 (1991).
5. J.-C. Lo, J. E. Johnson, C. W. Wuenschell, T. Saito, D. J. Anderson, *Genes Dev.* **5**, 1524 (1991).
6. C. Akazawa, M. Ishibashi, C. Shimizu, S. Nakanishi, R. Kageyama, *J. Biol. Chem.* **270**, 8730 (1995).
7. N. Ben-Arie *et al.*, *Hum. Mol. Genet.* **5**, 1207 (1996).
8. N. Ben-Arie *et al.*, *Nature* **390**, 169 (1997).
9. β-Gal targeting into the Math1 locus was carried out using the same homologous arms as previously described (*8*) with one small modification: the selectable marker for phosphoglycerokinase (PGK)–hypoxanthine phosphoribosyl-transferase was replaced with a β-Gal/PGK-neomycin cassette (*28*). This construct placed β-Gal in-frame with the Math1 start

Downloaded from www.sciencemag.org on June 29, 2010

codon. The same probes were used to identify targeted clones and genotyping.
10. N. Ben-Arie *et al.*, in preparation.
11. Pregnant females were culled, and embryos were dissected in ice-cold phosphate-buffered saline (PBS). The surrounding yolk sac was collected for genotyping. Embryos were fixed for 30 min in 4% paraformaldehyde/PBS then incubated in X-Gal (1 mg/ml) at 30°C for revealing β-Gal activity. Stained embryos were washed in PBS, postfixed for 1 hour in 4% paraformaldehyde/PBS, dehydrated, and either embedded in paraffin before sectioning or dissected to remove the inner ear for whole-mount studies.
12. N. A. Bermingham *et al.*, unpublished data.
13. LM and TEM were carried out as previously described (*29*). Tissue preparation for SEM consisted of treatment with 1% OsO_4 in cacodylate buffer, dehydration, critical-point drying, sputter coating with gold, and examination in a JEOL 35S electron microscope.
14. A. Rüsch, A. Lysakowski, R. A. Eatock, *J. Neurosci.* **18**, 7487 (1998).
15. M. Xiang *et al.*, *Proc. Natl. Acad. Sci. U.S.A.* **94**, 9445 (1997).
16. M. Xiang, W. Q. Gao, T. Hasson, J. J. Shin, *Development* **125**, 3935 (1998).
17. T. Hasson *et al.*, *J. Cell Biol.* **137**, 1287 (1997).
18. C. J. Dechesne, D. Rabejac, G. Desmadryl, *J. Comp. Neurol.* **346**, 517 (1994).
19. J. L. Zheng and W. Q. Gao, *J. Neurosci.* **17**, 8270 (1997).
20. For immunofluorescence, embryos were fixed for 1.5 hours in 4% paraformaldehyde/PBS at 4°C, sunk through 15% sucrose/PBS for 5 hours then through 30% sucrose/PBS overnight, and snap frozen in a 2-methylbutane dry ice bath. Fourteen-micrometer sections were cut on a cryostat and mounted on gelatin-coated slides. Sections were fixed on slides by dipping for 10 min in Streck tissue fixative (Streck Laboratories, Omaha, NE) and air drying. Sections were blocked in 10% normal goat serum and 0.3% Triton X-100 in PBS for 1 hour at room temperature (RT). Rabbit polyclonal antibody to calretinin (Chemicon International, Temecula, CA) was diluted 1:200 or rabbit antibody to myosin VI (a gift from T. Hasson, University of California, San Diego) was diluted 1:100 in blocking solution and incubated overnight on sections at 4°C. Sections were washed three times (20 min each) in PBS at RT. The secondary antibody, Alexa 488 (Molecular Probes, Eugene, OR), was diluted 1:400 in blocking solution. Sections were covered and incubated at RT for 2 hours before washing and mounting in Vectashield containing 4′6′-diamidino-2-phenylindole (DAPI) (Vector Laboratories, Burlingame, CA). For confocal microscopy, sections were treated with ribonuclease (25 μg/ml) before counterstaining with propidium iodide (50 μg/ml) and mounted in Vectashield without DAPI or were directly mounted in Vectashield containing TOTO-3 iodide (Molecular Probes). Stained sections were viewed under a Bio-Rad 1024 confocal microscope.
21. G. M. Cohen and C. D. Fermin, *Hear. Res.* **18**, 29 (1985).
22. M. J. Shiel and D. A. Cotanche, *ibid.* **47**, 147 (1990).
23. A. P. Jarman, Y. Grau, L. Y. Jan, Y. N. Jan, *Cell* **73**, 1307 (1993).
24. D. Eberl, personal communication.
25. B. A. Hassan and H. J. Bellen, unpublished observations.
26. C. Haddon, Y. J. Jiang, L. Smithers, J. Lewis, *Development* **125**, 4637 (1998); J. Adam *et al.*, *ibid.* **125**, 4645 (1998); P. Lanford *et al.*, *Nature Genet.* **21**, 289 (1999).
27. P. Kim, A. W. Helms, J. E. Johnson, K. Zimmerman, *Dev. Biol.* **187**, 1 (1997).
28. G. Friedrich and P. Soriano, *Genes Dev.* **5**, 1513 (1991).
29. A. Lysakowski and J. M. Goldberg, *J. Comp. Neurol.* **389**, 419 (1997)
30. We thank R. Atkinson, D. Trikka, and V. Brandt for assistance and helpful discussions and T. Hasson for the myosin VI antibody, and we acknowledge the support of the Electron Microscopic Facility of the University of Illinois Research Resources Center. N.A.B. and B.A.H. are associate fellows, H.J.B. is an Associate Investigator, and H.Y.Z. is an Investigator with the Howard Hughes Medical Institute. This work was partially supported by a grant from the National Institute on Deafness and Other Communication Disorders to R.A.E. and A.L. and by cores of the Mental Retardation Research Center at the Baylor College of Medicine.

14 December 1998; accepted 10 May 1999

Crystal Structure of the Zα Domain of the Human Editing Enzyme ADAR1 Bound to Left-Handed Z-DNA

Thomas Schwartz,[1] Mark A. Rould,[2] Ky Lowenhaupt,[1] Alan Herbert,[1] Alexander Rich[1]*

The editing enzyme double-stranded RNA adenosine deaminase includes a DNA binding domain, Zα, which is specific for left-handed Z-DNA. The 2.1 angstrom crystal structure of Zα complexed to DNA reveals that the substrate is in the left-handed Z conformation. The contacts between Zα and Z-DNA are made primarily with the "zigzag" sugar-phosphate backbone, which provides a basis for the specificity for the Z conformation. A single base contact is observed to guanine in the syn conformation, characteristic of Z-DNA. Intriguingly, the helix-turn-helix motif, frequently used to recognize B-DNA, is used by Zα to contact Z-DNA.

Since the elucidation of the structure of left-handed Z-DNA in 1979 (*1*), the question of a biological role for this conformation has remained in the forefront of research in the field. The discovery of a Z-DNA binding activity for double-stranded (ds) RNA adenosine deaminase (ADAR1) constituted an important step (*2*). ADAR1 deaminates adenine in pre-mRNA, yielding inosine, which codes as guanine. Such codon changes result in alternative forms of the translated protein. The NH_2-terminus of ADAR1 includes a domain, Zα, which is responsible for high-affinity binding to the Z conformation of DNA. This was originally shown by a band-shift assay (*3*), where the binding withstood a challenge of a 10,000-fold mass excess of nonspecific B-DNA competitor (*2, 4*). Circular dichroic and Raman spectroscopic measurements have confirmed the specificity of Zα containing peptides for Z-DNA (*4–6*). Zα is the prototype for a family of related peptides, which share common amino acid sequence motifs (*4*). We have now cocrystallized a proteolytically defined Zα domain [residues 133 to 209 (*7, 8*)] of human ADAR1 with the 6–base pair (bp) DNA fragment $d(TCGCGCG)_2$. The structure was determined by single isomorphous replacement including anomalous scattering (SIRAS) and was refined to a resolution of 2.1 Å (Table 1).

The monomeric Zα domain binds to one strand of the palindromic dsDNA. The conformation of the DNA substrate is very similar to the canonical Z-DNA structure determined by Wang *et al.* (*1, 9*) [root mean square deviation (rmsd) 0.80 Å, including all atoms in the duplex]. A second monomer related by the twofold axis of the DNA oligomer binds to the opposite strand of the DNA; however, the two proteins do not interact with each other. In the asymmetric unit there are three independent Zα-DNA complexes (*10*).

The Zα domain has a compact α/β architecture containing a three-helix bundle (α1 to α3) flanked on one side by a twisted antiparallel β sheet (β1 to β3) (Fig. 1). The NH_2-terminal helix α1 (Ser^{134} to Leu^{150}) is followed by the short-strand β1 (Ala^{155} to Thr^{157}), which positions the COOH-terminal β hairpin (β2: Leu^{185} to Ala^{188}; β3: Pro^{193} to Ile^{197}) by means of two hydrogen bonds. This arrangement of a β hairpin with exactly two hydrogen bonds to a third β strand is a common feature of helix-turn-helix (HTH) proteins with α/β topology. Helices α2 and α3 (Ala^{158} to Leu^{165} and Lys^{169} to Lys^{182}) reside between β1 and β2 and form the HTH motif. Aliphatic residues from the three helices, together with Trp^{195} in strand β3, interdigitate and form a hydrophobic core. The secondary structure reported in a nuclear magnetic resonance experiment indicates that the unbound protein in solution adopts a very similar fold (*11*).

[1]Department of Biology, Massachusetts Institute of Technology, Cambridge, MA 02139, USA. [2]Department of Molecular Physiology and Biophysics, University of Vermont, Burlington, VT 05405, USA.

*To whom correspondence should be addressed.

Downloaded from www.sciencemag.org on June 29, 2010